nature chemical biology

ARTICLES

https://doi.org/10.1038/s41589-019-0327-1

Programmable RNA N^6-methyladenosine editing by CRISPR-Cas9 conjugates

Xiao-Min Liu[1], Jun Zhou[1,2], Yuanhui Mao[1], Quanquan Ji[1] and Shu-Bing Qian[1*]

RNA modification in the form of N^6-methyladenosine (m^6A) regulates nearly all the post-transcriptional processes. The asymmetric m^6A deposition suggests that regional methylation may have distinct functional consequences. However, current RNA biology tools do not distinguish the contribution of individual m^6A modifications. Here we report the development of 'm^6A editing', a powerful approach that enables m^6A installation and erasure from cellular RNAs without changing the primary sequence. We engineered fusions of CRISPR-Cas9 and a single-chain m^6A methyltransferase that can be programmed with a guide RNA. The resultant m^6A 'writers' allow functional comparison of single site methylation in different messenger RNA regions. We further engineered m^6A 'erasers' by fusing CRISPR-Cas9 with ALKBH5 or FTO to achieve site-specific demethylation of RNAs. The development of programmable m^6A editing not only expands the scope of RNA engineering, but also facilitates mechanistic understanding of epitranscriptome.

Reversible RNA modification forms the epitranscriptomic code that regulates gene expression beyond the primary sequence[1,2]. In eukaryotic cells, the most abundant internal RNA modification is N^6-methyladenosine (m^6A). m^6A installation on RNA is mediated by a methyltransferase complex consisting of core subunits METTL3, METTL14, WTAP and other proteins such as KIAA1429 and RBM15 (refs. [3–5]). This m^6A 'writer' recognizes the consensus sequence RRACH (R, purine and H, non-guanine base), although not all the consensus sequences are methylated. The finding that FTO and ALKBH5 exhibit the demethylation activity toward m^6A suggests the dynamic feature of m^6A modification[6,7]. The m^6A mark is decoded by specific 'readers' to mediate a variety of downstream effects on RNA metabolism[8,9]. A recent study further reported that m^6A repels certain RNA-binding proteins[10], forming an additional layer in controlling dynamic RNA–protein interaction. Despite the tremendous progress in the functional characterization of m^6A modification, the regional effects of methylation on messenger RNA remain obscure. In particular, m^6A takes on an asymmetric distribution along mRNA with the majority of methylation clustered near the stop codon[11,12]. Recent m^6A-seq studies also revealed m^6A peaks in 5′ untranslated regions (UTR) and start codons when plotting the peak density along the transcriptome. However, current RNA biology tools do not distinguish the contributions of individual m^6A modifications, imposing a substantial barrier to our understanding of the mechanism by which m^6A markers influence cellular activities.

Recent advances in CRISPR-based technologies have revolutionized biomedical research by enabling precision genome editing[13–15]. From targeted DNA cleavage/repair to direct base editing, genetic components can be engineered with high efficiency and specificity. Gene expression is also subjected to regulation by DNA methylation and histone modifications (the 'epigenome')[16,17]. By fusing catalytically dead Cas9 (dCas9) to DNA or histone modifying enzymes, site-specific epigenome engineering becomes possible[18,19]. With the availability of Cas proteins capable of targeting single-stranded RNA[20,21], programmable editing of epitranscriptome by coupling RNA-targeting Cas with RNA base-modifying enzymes would be attractive. However, such implementation is held back by several challenges. First, our knowledge about the RNA modification machinery remains rudimentary. Second, a direct sequencing method for quantitative profiling of site-specific RNA base modifications is still lacking. Third, the complex physiological effect of RNA modifications hinders functional interpretation of engineered epitranscriptome. In the case of m^6A modification, it is unclear whether particular outcomes require a single RNA methylation event or an ensemble of m^6A modifications that function as a synergistic unit.

Here we report the development of 'm^6A editing', a powerful approach that enables m^6A installation and erasure from cellular RNAs without changing the primary sequence. We created engineered m^6A 'writers' by fusing CRISPR-Cas9 and a single-chain m^6A methyltransferase. We further engineered m^6A 'erasers' by fusing CRISPR-Cas9 with full-length ALKBH5 or FTO to achieve site-specific demethylation of RNAs. The resultant m^6A editors can be programmed with a guide RNA, allowing functional comparison of single site methylation in different mRNA regions.

Results

Designing programmable m^6A writers. Much of our knowledge of m^6A is built on genetic perturbations of modifying enzymes that have pleiotropic effects on cellular physiology. It also inevitably affects global RNA methylation. To interrogate the regional effect of m^6A, current methods often rely on point mutations that permanently remove the modification site from the transcript of interest. However, the altered nucleotide sequence may introduce unwanted properties and complicate data interpretation. It is thus highly desirable to develop a method that can manipulate individual m^6A modifications at specific sites of individual transcripts without changing the primary sequence. We attempted to engineer the m^6A machinery into a programmable RNA base modifier by taking advantage of RNA-guided dCas9 (refs. [20,21]). m^6A is installed on RNA molecules by a MTase complex comprising METTL3, METTL14 and WTAP via recognition of the consensus sequence RRACH (R, purine; H, non-guanine base)[8,9]. Structural studies revealed that METTL3 pri-

[1]Division of Nutritional Sciences, Cornell University, Ithaca, NY, USA. [2]Present address: School of Life Science and Technology, China Pharmaceutical University, Nanjing, China. *e-mail: sq38@cornell.edu

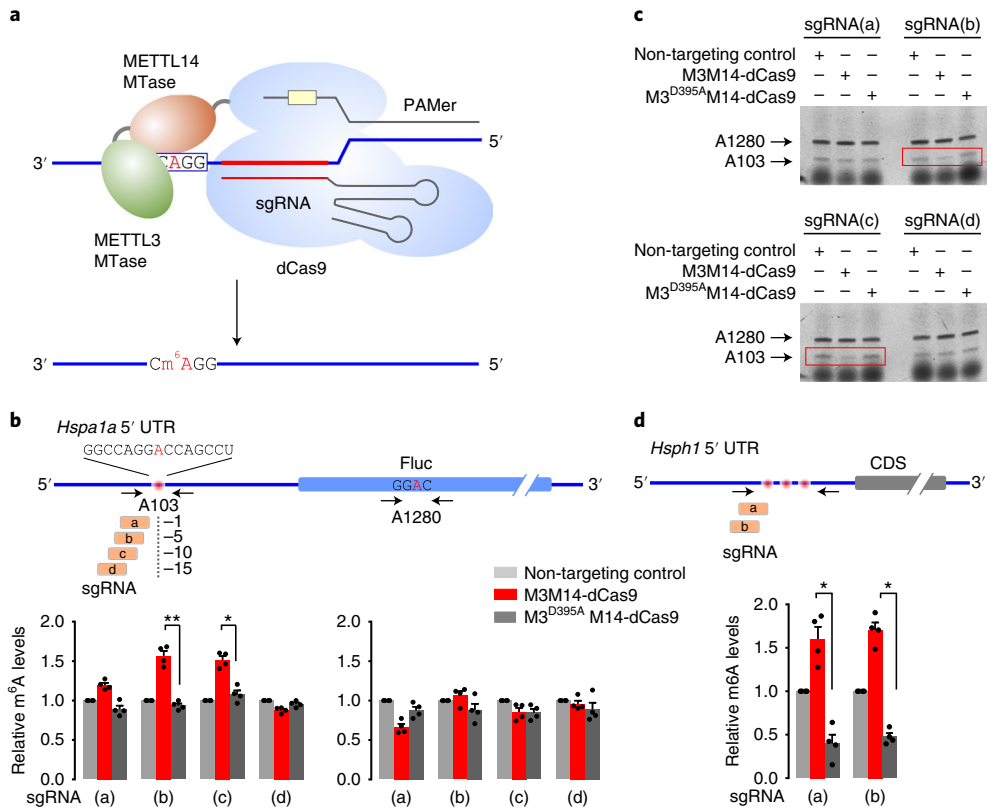

Fig. 1 | Targeted 5′ UTR methylation by engineered m⁶A 'writers' a, Schematic of engineered m⁶A 'writers' by coupling CRISPR-dCas9 with single-chain methyltransferase domains derived from METTL3 (green) and METTL14 (brown). The sgRNA and PAMmer are base-paired to nearby regions of the m⁶A consensus motif on target RNA. PAMer supplies the PAM sequence NGG that does not need to be present on target RNA. **b**, Measurement of m⁶A levels on *Hspa1a* 5′ UTR-Luc in transfected HeLa cells. λ2 sgRNA was used as the non-targeting control. Primers were designed to span the targeting m⁶A site A103 in *Hspa1a* 5′ UTR or A1280 of Fluc mRNA as control for off-targeting. Error bars, mean ± s.e.m.; unpaired Student's *t*-test, $^*P < 0.05$, $^{**}P < 0.01$; $n = 4$ independent experiments. **c**, Site-specific detection of m⁶A on *Hspa1a* 5′ UTR-Luc in transfected HeLa cells using fluorescein-dUTP-incorporated primer-extension approach. Both specific (A103) and non-specific (A1280) sites were detected from the same sample. Red boxes highlight decreased probe +1 signals as a result of increased methylation by M3M14-dCas9 but not the inactive mutant. This experiment was repeated twice with similar results. Uncropped scans are shown in Supplementary Fig. 11. **d**, Measurement of m⁶A levels on endogenous *Hsph1* 5′ UTR in MEF cells transfected with engineered m⁶A 'writers'. λ2 sgRNA was used as the non-targeting control. Error bars, mean ± s.e.m.; unpaired Student's *t*-test, $^*P < 0.05$; $n = 4$ independent experiments.

marily functions as the catalytic core, while METTL14 serves as an RNA-binding platform[22,23]. Since the METTL3-METTL14 heterodimer possesses strong catalytic activity, we constructed a single-chain m⁶A MTase by linking two MTase domains derived from human METTL3 and METTL14, respectively (Fig. 1a). We expressed and purified two fusion proteins with different orientations of MTase domains. In vitro methyltransferase assay showed that M3M14 exhibited more than three-fold higher catalytic activity than M14M3 (Supplementary Fig. 1a). Consistent with the previous finding that AdoMet binds to the DPPW motif of METTL3 (refs. [22,23]), introducing D395A mutation abolished the catalytic activity of both recombinant proteins (Supplementary Fig. 1a).

We next fused M3M14 to the amino terminus of dCas9 using the same linker designed for the DNA base editor (Supplementary Fig. 1b)[24]. Unlike the endogenous METTL3 or METTL14, which are primarily localized in the nucleus, both M3M14-dCas9 and M3^{D395A}M14-dCas9 fusion proteins showed predominant cytosolic localization in transfected human embryonic kidney (HEK)293T and mouse embryonic fibroblast (MEF) cells (Supplementary Fig. 1c,d). Although physiological m⁶A modification occurs on nascent RNAs in a co-transcriptional manner[25], the cytosolic presence of engineered m⁶A 'writers' offers an attractive approach to targeting mature RNAs for de novo methylation. Similar to DNA-targeting dCas9, RNA-targeting dCas9 requires sequence-specific guide RNA (sgRNA) and the protospacer adjacent motif (PAM) supplied by an antisense oligonucleotide (PAMer) (Fig. 1a). Consistent with the previous report[20], we found that PAMer is essential for efficient binding of M3M14-dCas9 to the target RNA (Supplementary Fig. 2a). With two regional base pairing conferred by sgRNA and PAMer, possible off-targeting of dCas9 can be minimized, thereby increasing the specificity of RNA targeting.

Programmable 5′ UTR m⁶A modification. To assess whether M3M14-dCas9 is capable of inducing site-specific m⁶A modification, we first designed sgRNAs targeting the 5′ UTR of Hsp70 mRNA. Since the level of endogenous *Hspa1a* is undetectable in MEF cells under the normal growth condition, we introduced a firefly luciferase (Fluc) reporter bearing the 5′ UTR of *Hspa1a* (Fig. 1b). In transfected MEF cells, the exogenous 5′ UTR exhibited basal m⁶A modification at A103 as evidenced by quantitative PCR with reverse transcription (RT–qPCR) of methylated RNA fragments enriched by m⁶A antibodies (m⁶A-RIP). This modification represents a genuine m⁶A mark because it is highly sensitive to METTL3 knockdown (Supplementary Fig. 2b). To test whether M3M14-dCas9 can further boost the m⁶A signal at this position, we designed a panel of four sgRNAs with their 5′ ends located at varied distances to A103 (Fig. 1b). Overexpression of M3M14-dCas9 alone had negligible effect on total RNA methylation (Supplementary Fig. 2c).

However, co-transfection of sgRNA and PAMer resulted in site-specific m^{6}A modification at A103 of *Hspa1a*-Fluc with varied efficiencies (Fig. 1b). We observed a >50% increase of m^{6}A signals for sgRNA(b) and sgRNA(c), suggesting an effective window of ~10 nucleotides for targeted methylation. This is consistent with the flexible nature of the XTEN linker between M3M14 and dCas9. The increased methylation was due to the catalytic activity of the engineered m^{6}A 'writer' because little methylation was observed on expression of M3^{D395A}M14-dCas9. The induced m^{6}A modification was site-specific because a putative m^{6}A site at the coding region of Fluc (A1280) showed comparable methylation signals regardless of the sgRNA presented (Fig. 1b, right panel).

m^{6}A-RIP coupled with RT–qPCR, albeit quantitative, does not offer single nucleotide resolution. A sequencing-based approach, miCLIP, provides single nucleotide m^{6}A mapping but lacks quantitative features[26]. To circumvent these limitations, we devised site-specific m^{6}A quantification by coupling m^{6}A antibody crosslinking with probe elongation[27]. We validated this approach by using synthetic RNAs containing A or m^{6}A at specific positions (Supplementary Fig. 2d). When *Hspa1a*-Fluc was examined from transfected cells, we observed an evident reduction of the 'probe+1' signal at A103 in the presence of sgRNA(b) or sgRNA(c) (Fig. 1c). Since a decreased 'probe+1' signal is an indication of increased methylation events, this result is in agreement with m^{6}A-RIP. The same transcripts showed little difference in probe extension at A1280, a putative m^{6}A site in the Fluc coding region. Finally, neither the control sgRNA nor the inactive M3^{D395A}M14-dCas9 altered the level of 'probe+1' signals. As an independent validation, we applied a non-antibody-based methodology to quantify the site-specific m^{6}A editing. The recently reported SELECT method exploits the ability of m^{6}A to hinder the single-base elongation activity of DNA polymerases and the nick ligation efficiency of ligases[28] (Supplementary Fig. 3a). Consistent with the antibody-based results, SELECT revealed quantitative reduction of ligated products for the targeted A103 of *Hspa1a*, but not the Fluc A1280 (Supplementary Fig. 3b). These results collectively confirmed that M3M14-dCas9 is able to achieve sgRNA-guided site-specific m^{6}A modification.

We noticed that, for Hsp70 5′ UTR, the targeted m^{6}A modification efficiency is relatively low. This could be due to the high basal level of methylation at this position that limits the extent of further increase. We next chose the 5′ UTR from Hsp105 that has relatively low methylation levels in MEFs as evidenced by m^{6}A-seq (Supplementary Fig. 4a). Further, knocking down the methyltransferase METTL3 had limited effect on the level of methylation. By contrast, silencing the demethylase FTO significantly increased the steady-state m^{6}A levels in the 5′ UTR of Hsp105 (Supplementary Fig. 4b). Notably, the 5′ UTR of Hsp105 contains a cluster of putative m^{6}A sites, which could be targeted by the same sgRNA. We constructed a Fluc reporter bearing the mouse Hsp105 5′ UTR and designed two sgRNAs targeting the m^{6}A cluster. In transfected HeLa cells, two sgRNAs each induced ~two-fold increase of 5′ UTR methylation catalyzed by M3M14-dCas9 but not the inactive M3^{D395A}M14-dCas9 (Supplementary Fig. 4c). Once again, the non-targeted m^{6}A site (A1280) of the same transcript showed little difference of methylation, confirming the specificity of programmable m^{6}A modification. This encouraging result prompted us to examine whether the engineered m^{6}A 'writer' is able to target the endogenous transcript in MEF cells. This was indeed the case as the same sgRNAs significantly increased the 5′ UTR methylation of *Hsph1* in transfected MEFs (Fig. 1d).

Effects of targeted 5′ UTR m^{6}A modification. The 5′ UTR is crucial for ribosome scanning and it is unclear whether the binding of CRISPR-Cas9 system in the 5′ UTR would interfere with the normal translation process (Fig. 2a). A previous study reported that CRISPR-Cas9 targeting 5′ UTR or the coding region inhibited mRNA translation by acting as a roadblock[29]. Using the Fluc reporter assay, we found that the presence of sgRNA or PAMer alone does not seem to block the ribosome scanning process despite the sequence complementarity to the 5′ UTR of Hsp105 (Supplementary Fig. 5a). Additionally, co-transfection with M3M14-dCas9 had negligible effect on Fluc levels, at least under the normal growth condition (Supplementary Fig. 5b). We previously reported that 5′ UTR methylation in the form of m^{6}A enables cap-independent translation under stress conditions[30,31]. We next subjected the transfected cells to heat shock stress at 42 °C for 1 h, which denatured preexisting Fluc. During stress recovery, we observed an increased Fluc levels in the presence of M3M14-dCas9 when compared to the inactive mutant (Fig. 2b). The steady-state levels of Fluc mRNA were comparable, suggesting a translational effect. The same phenomenon holds true for Hsp70 5′ UTR (Fig. 2b). These results support the notion that 5′ UTR m^{6}A promotes non-canonical translation when the cap-dependent mechanism is repressed.

Accumulating evidence suggests the role of m^{6}A modification in promoting mRNA degradation[32]. However, it is unclear whether the m^{6}A mark installed at different regions exhibits distinct effects. Programmable m^{6}A 'writing' permits functional dissection of site-specific effects of methylation without introducing point mutations. We first assessed the effect of 5′ UTR methylation on mRNA stability by taking advantage of Fluc mRNAs bearing Hsp105 5′ UTR. To evaluate the turnover rate of Fluc mRNA, we treated transfected cells with the transcription inhibitor actinomycin D for various times followed by RT–qPCR. Despite the two-fold increase of m^{6}A in 5′ UTR catalyzed by M3M14-dCas9 (Supplementary Fig. 4c), we observed little difference of mRNA turnover (Supplementary Fig. 5c). Similarly, Hsp70 5′ UTR had no effects on the stability of Fluc mRNA regardless of the methylation status (Supplementary Fig. 5d). The negligible effect of 5′ UTR methylation on mRNA turnover could be due to the eviction of potential m^{6}A 'readers' by the scanning ribosome.

Programmable 3′ UTR m^{6}A modification. We next examined whether 3′ UTR methylation induced by the engineered m^{6}A 'writers' could promote mRNA degradation. The abundant β-actin mRNA contains a well-defined m^{6}A site after the stop codon (A1216) and the moderate methylation levels (21% in HeLa cells) provide room for further m^{6}A installation (Supplementary Fig. 6a)[33]. Supporting this notion, overexpression of METTL3 resulted in a 50% increase of m^{6}A at this position as measured by m^{6}A-RIP (Supplementary Fig. 6b). To examine whether a single site m^{6}A modification in the 3′ UTR contributes to the degradation of *Actb*, we designed two sgRNAs and corresponding PAMers targeting A1216 (Fig. 2c). In transfected HeLa cells, only sgRNA(a) increased the methylation at A1216 (~three-fold) as quantified by m^{6}A-RIP (Fig. 2c). As an independent validation, we conducted site-specific m^{6}A quantification. Indeed, only sgRNA(a) reduced the 'probe+1' signal at A1216 of β-actin mRNA, corresponding to the increased methylation (Fig. 2d). Notably, the same sample showed little difference of methylation at A2577 of *Malat1*, a non-coding RNA as a non-targeting internal control (Fig. 2d). To substantiate the targeting specificity of m^{6}A modification by the engineered m^{6}A writer, we applied SELECT to the same samples and observed significant reduction of ligated products by sgRNA(a), an indication of increased m^{6}A levels (Supplementary Fig. 6c).

Although ectopic expression of M3M14-dCas9 does not seem to alter global RNA methylation (Supplementary Fig. 2c), it is unclear whether the presence of particular sgRNAs leads to off-targeting of m^{6}A methylation. To assess the off-targeting possibility of *Actb*-specific sgRNA(a) across the transcriptome, we conducted optimized m^{6}A-seq. With improved resolution (Supplementary Fig. 7a,b), we compared the entire m^{6}A methylome in cells expressing active or inactive m^{6}A writer, in the presence of targeted sgRNA

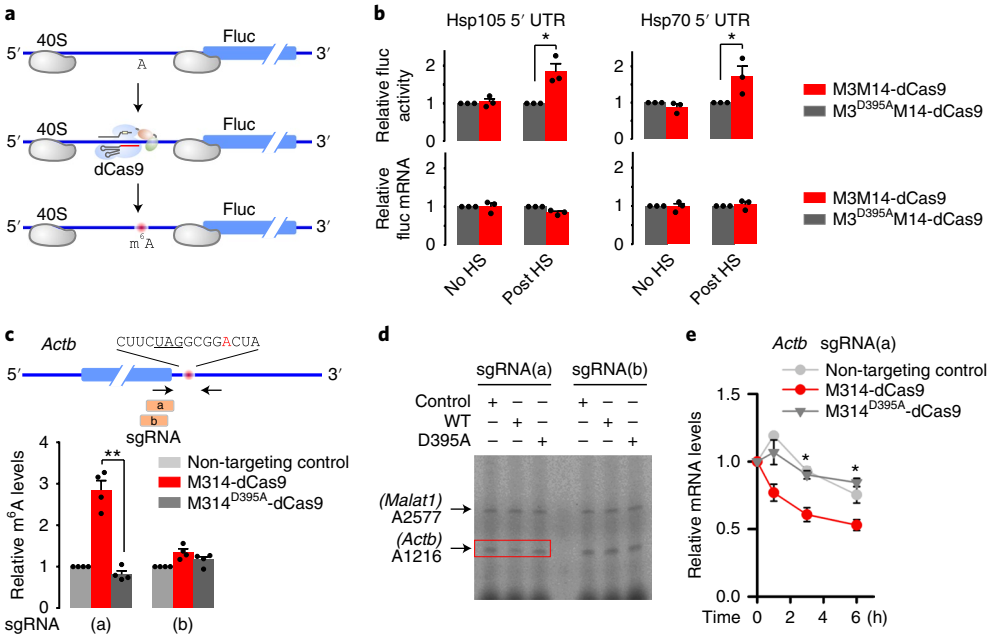

Fig. 2 | Physiological effects of targeted methylation by engineered m⁶A 'writers' a, The panel shows possible effects of 5 UTR m⁶A 'writers' on ribosome scanning and subsequent translation. **b**, Translational effects of targeted 5′ UTR m⁶A modification in transfected HeLa cells before and after heat shock (42 °C for 1h). Fluc activities were monitored during heat shock (HS) stress recovery. Fluc mRNA levels were also measured in parallel. Error bars, mean ± s.e.m.; unpaired Student's *t*-test, $^{*}P < 0.05$; $n = 3$ independent experiments. **c**, Measurement of m⁶A levels on endogenous *Actb* 3′ UTR in HeLa cells transfected with engineered m⁶A 'writers'. λ2 sgRNA was used as the non-targeting control. Primers were designed to span the targeting m⁶A site at A1216 of *Actb* 3′ UTR. Error bars, mean ± s.e.m.; unpaired Student's *t*-test, $^{**}P < 0.01$; $n = 4$ independent experiments. **d**, Site-specific detection of m⁶A on endogenous *Actb* in transfected HeLa cells using fluorescein-dUTP-incorporated primer-extension approach. In addition to the specific site (A1216) of *Actb*, the non-specific site (A2577 of *Malat1*) from the same sample was used as negative control. Red boxes highlight decreased probe+1 signals as a result of increased methylation by M3M14-dCas9 but not the inactive mutant. This experiment was repeated three times with similar results. Uncropped scans are shown in Supplementary Fig. 11. **e**, Measurement of *Actb* decay in HeLa cells transfected with engineered m⁶A 'writers'. Then, 36 h after transfection, cells were treated with actinomycin D for various times before sample collection for RT-qPCR. Error bars, mean ± s.e.m.; unpaired Student's *t*-test, $^{*}P < 0.05$; $n = 3$ independent experiments.

or λ2 sgRNA control. The overall m⁶A landscapes across the transcriptome are comparable in these cells (Supplementary Fig. 7c). Pair-wise comparison of individual m⁶A sites showed limited variation (Supplementary Fig. 7d). The targeted site of *Actb* showed an evident increase of m⁶A density in cells expressing M3M14-dCas9 when compared to the inactive mutant (Supplementary Fig. 7e). Although different sgRNAs could have different outcomes, the possible off-target of sgRNA-guided m⁶A writers is either negligible or beyond the detection threshold.

Having achieved site-specific 3′ UTR m⁶A modification of β-actin mRNA by sgRNA(a), we next examined the stability of endogenous *Actb* in these cells. The half-life of *Actb* was significantly reduced in the presence of MTase-dCas9, but not MTase^{D395A}-dCas9 (Fig. 2e). Notably, the non-targeted transcript *Gapdh* maintained its stability in the same samples (Supplementary Fig. 7f). The correlation between sgRNA(a)-guided m⁶A installation and increased mRNA turnover suggests that a single m⁶A modification at 3′ UTR influences the mRNA stability.

Designing programmable m⁶A erasers. To fully interrogate the regional effect of m⁶A modification, it is highly desirable to achieve targeted erasure of m⁶A from mRNA using engineered demethylases. Two members of the α-ketoglutarate-dependent dioxygenases protein family, FTO and ALKBH5, have been shown to act as m⁶A demethylases[6,7]. Unlike m⁶A 'writers' that require consensus motif for targeting, the substrate specificity of ALKBH5 and FTO seems to rely on conformational markers signified by m⁶A[34]. In addition to internal m⁶A, FTO can also demethylase m⁶Am adjacent to the 5′ end cap[35,36]. Since the non-AlkB domains are crucial in the functionality of both demethylases, we fused the full-length ALKBH5 or FTO to the amino terminus of dCas9 (Fig. 3a). To generate inactive controls, we introduced H204A mutation to ALKBH5 and (H231A, D233A) double mutations to FTO (Supplementary Fig. 8a,d). These fusion proteins primarily localized in the nucleus of transfected cells as expected (Supplementary Fig. 8b,e). Notably, overexpression of these engineered 'erasers' alone did not alter global m⁶A levels in transfected cells (Supplementary Fig. 8c,f). To assess the off-targeting effect, we conducted optimized m⁶A-seq and compared the entire m⁶A methylome in cells expressing active or inactive FTO-dCas9, in the presence of targeted sgRNA or λ2 sgRNA control. The overall m⁶A landscapes across the transcriptome are comparable in these cells (Supplementary Fig. 9a). Pair-wise comparison of individual m⁶A sites showed that the global variation in the presence of targeted sgRNA is no greater than the control (Supplementary Fig. 9b).

To evaluate the sgRNA-guided demethylation activity of ALKBH5-dCas9 and FTO-dCas9, we chose to target *Malat1* because this abundant long non-coding RNA exhibits a high degree of methylation at A2577 (80% in HeLa cells) (Supplementary Fig. 10a)[33]. We designed two sgRNAs and corresponding PAMers targeting A2577 of *Malat1*. Only sgRNA(a) was able to reduce its methylation when co-expressed with either ALKBH5-dCas9 or FTO-dCas9 (Fig. 3b). This was due to the demethylase activity of engineered m⁶A erasers because inactive mutants of ALKBH5 did not alter the m⁶A signal at A2577 of *Malat1* (Fig. 3c). The m⁶A levels at A1216 of *Actb* were comparable in the presence of sgRNA(a) targeting *Malat1*. The high specificity of ALKBH5-dCas9 was further confirmed using

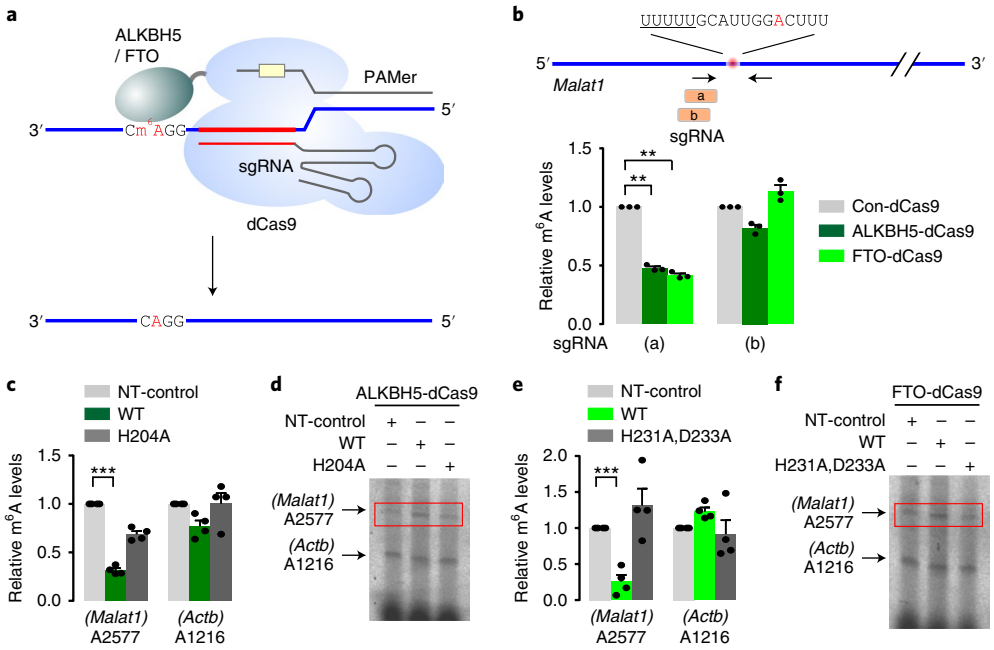

Fig. 3 | Targeted RNA demethylation by engineered m⁶A 'erasers' a, Schematic of engineered m⁶A 'erasers' by coupling CRISPR-dCas9 with full-length ALKBH5 or FTO. The sgRNA and PAMmer are base paired to nearby regions of the m⁶A site on target RNA. PAMer supplies the PAM sequence NGG that does not need to be present on target RNA. **b**, Measurement of m⁶A levels on endogenous *Malat1* in HeLa cells transfected with engineered m⁶A 'erasers'. Primers were designed to span the highly methylated m⁶A site A2577 in *Malat1*. Error bars, mean ± s.e.m.; unpaired Student's *t*-test, $^{**}P < 0.01$; $n = 3$ independent experiments. **c**, Measurement of m⁶A levels on A2577 of *Malat1* and A1216 of *Actb* in HeLa cells transfected with active or inactive ALKBH5-dCas9 in the presence of sgRNA(a). Error bars, mean ± s.e.m.; unpaired Student's *t*-test, $^{***}P < 0.001$; $n = 4$ independent experiments. NT-control indicates non-targeting sgRNA control; WT, wild type. **d**, Site-specific detection of m⁶A using the same samples as **c**. Red boxes highlight increased probe +1 signals as a result of reduced methylation by ALKBH5-dCas9 but not the inactive mutant. This experiment was repeated twice with similar results. Uncropped scans are shown in Supplementary Fig. 11. **e**, Measurement of m⁶A levels on A2577 of *Malat1* and A1216 of *Actb* in HeLa cells transfected with active or inactive FTO-dCas9 in the presence of sgRNA(a). Error bars, mean ± s.e.m.; unpaired Student's *t*-test, $^{***}P < 0.001$; $n = 4$ independent experiments. **f**, Site-specific detection of m⁶A using the same samples as **e**. Red boxes highlight increased probe+1 signals as a result of reduced methylation by FTO-dCas9 but not the inactive mutant. This experiment was repeated twice with similar results. Uncropped scans are shown in Supplementary Fig. 11.

site-specific m⁶A quantification (Fig. 3d). The same finding holds true for FTO-dCas9 (Fig. 3e,f), validating the specificity of programmable m⁶A erasers.

m⁶A editing of *Malat1* acts as a structural switch. Only sgRNA(a) enables site-specific *Malat1* demethylation. To substantiate this finding further, we employed the SELECT analysis and confirmed the differential effect between sgRNA(a) and sgRNA(b) (Fig. 4a,b). m⁶A at A2577 has been reported to act as a structural switch for *Malat1* by destabilizing the stem structure[37]. As a result, the exposed U-tract allows subsequent binding of heterogeneous nuclear ribonucleoprotein C (HNRNPC) (Fig. 4c and Supplementary Fig. 10b). Since sgRNA(b) is located upstream of the U-tract, it is possible that the presence of HNRNPC prevents the access of engineered m⁶A 'erasers' to the target site. As an independent means to evaluate the methylation status of *Malat1*, we conducted HNRNPC immunoprecipitation coupled with RT–qPCR of *Malat1*. Once again, only sgRNA(a) significantly reduced the *Malat1*-associated HNRNPC (Fig. 4c), confirming the functional consequence of m⁶A erasure from A2577 of *Malat1*. This result indicates that m⁶A editing has the potential to control interactions of RNA-binding proteins by remodeling RNA structures. The comparable catalytic activities between ALKBH5-dCas9 and FTO-dCas9 also indicate that FTO is capable of targeting internal m⁶A.

Discussion

A challenge in the post-genomic era has been to elucidate the complex layers of epigenetic control of gene expression. Over the past 30 years, much research has been conducted on how DNA methylation and histones modifications (the 'epigenome') regulate gene expression[16,17]. More recently, RNA modifications have been discovered that decorate all RNA species across many living organisms. Dynamic and reversible RNA modifications constitute the 'epitranscriptome', a tunable layer influencing nearly all aspects of RNA metabolism and functionality[1,2]. Much of our current knowledge about RNA post-transcriptional modifications is limited to studies that rely on genetic perturbations that affect global RNA methylation as a whole. Although these results are informative for implicating the significance of RNA markers in cellular regulation, they are too limited for detailed mechanistic dissection. Additionally, the asymmetric m⁶A deposition suggests that regional methylation may have distinct functional consequences. To interrogate the site-specific effect of m⁶A, point mutation is a common methodology to permanently remove the modification site. However, we lack an approach to m⁶A installation in a site-specific manner.

By coupling CRISPR-Cas9 technology, the m⁶A editors described here offer researchers a versatile toolbox to unlock the secrets of epitranscriptome. It is now possible to achieve site-specific m⁶A installation or erasure, which is key to understanding the regional effects of mRNA methylation. We confirmed that a single site 5′ UTR methylation enables non-canonical mRNA translation. By contrast, manipulating 3′ UTR methylation influences mRNA turnover but not in an exclusive manner. One important application of m⁶A editing is to alter RNA secondary structures without changing the primary sequence. By site-specific m⁶A editing, certain m⁶A-dependent RNA structural switches can now be remodeled, offering

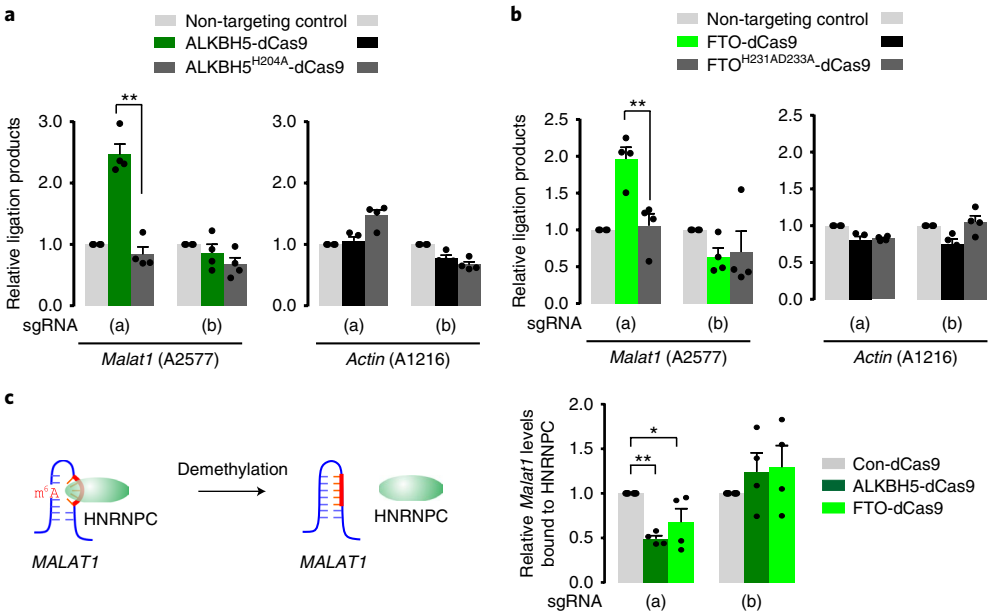

Fig. 4 | Physiological effects of targeted demethylation by engineered m^{6}A 'erasers' a, Measurement of m^{6}A levels on A2577 of *Malat1* and A1216 of *Actb* in HeLa cells transfected with active or inactive ALKBH5-dCas9 in the presence of sgRNA(a) and sgRNA(b). Error bars, mean ± s.e.m.; unpaired Student's *t*-test, $^{**}P < 0.01$; $n = 4$ independent experiments. **b**, Measurement of m^{6}A levels on A2577 of Malat1 and A1216 of Actb in HeLa cells transfected with active or inactive FTO-dCas9 in the presence of sgRNA(a) and sgRNA(b). Error bars, mean ± s.e.m.; unpaired Student's *t*-test, $^{**}P < 0.01$; $n = 4$ independent experiments. **c**, The left panel depicts the binding of HNRNPC to the U-tract of *Malat1* in the presence of m^{6}A. Lack of m^{6}A modification leads to HNRNPC dissociation. The right panel shows relative levels of *Malat1* bound to HNRNPC in HeLa cells transfected with engineered m^{6}A 'erasers'. Error bars, mean ± s.e.m.; unpaired Student's *t*-test, $^{*}P < 0.05$, $^{**}P < 0.01$; $n = 4$ independent experiments.

a powerful approach to fine-tuning specific RNA-protein interactions. With the versatility of CRISPR-Cas enzymes on the rise[15], it is conceivable to construct m^{6}A editors with smaller size, higher specificity and more adjustable features such as the one inducible by small molecules. Given the broad range of chemical modifications in cellular RNAs, our approach also serves as a prototype for developing toolkits capable of editing diverse base or sugar modifications of RNA molecules.

Online content

Any methods, additional references, Nature Research reporting summaries, source data, statements of code and data availability and associated accession codes are available at https://doi.org/10.1038/s41589-019-0327-1.

Received: 6 May 2018; Accepted: 23 June 2019;
Published online: 5 August 2019

References

1. Roundtree, I. A., Evans, M. E., Pan, T. & He, C. Dynamic RNA modifications in gene expression regulation. *Cell* **169**, 1187–1200 (2017).
2. Lewis, C. J., Pan, T. & Kalsotra, A. RNA modifications and structures cooperate to guide RNA-protein interactions. *Nat. Rev. Mol. Cell Biol.* **18**, 202–210 (2017).
3. Bokar, J. A., Shambaugh, M. E., Polayes, D., Matera, A. G. & Rottman, F. M. Purification and cDNA cloning of the AdoMet-binding subunit of the human mRNA (N6-adenosine)-methyltransferase. *RNA* **3**, 1233–1247 (1997).
4. Liu, J. et al. A METTL3-METTL14 complex mediates mammalian nuclear RNA N6-adenosine methylation. *Nat. Chem. Biol.* **10**, 93–95 (2014).
5. Ping, X. L. et al. Mammalian WTAP is a regulatory subunit of the RNA N6-methyladenosine methyltransferase. *Cell Res.* **24**, 177–189 (2014).
6. Jia, G. et al. N6-methyladenosine in nuclear RNA is a major substrate of the obesity-associated FTO. *Nat. Chem. Biol.* **7**, 885–887 (2011).
7. Zheng, G. et al. ALKBH5 is a mammalian RNA demethylase that impacts RNA metabolism and mouse fertility. *Mol. Cell* **49**, 18–29 (2013).
8. Fu, Y., Dominissini, D., Rechavi, G. & He, C. Gene expression regulation mediated through reversible m(6)A RNA methylation. *Nat. Rev. Genet.* **15**, 293–306 (2014).
9. Meyer, K. D. & Jaffrey, S. R. The dynamic epitranscriptome: N6-methyladenosine and gene expression control. *Nat. Rev. Mol. Cell Biol.* **15**, 313–326 (2014).
10. Edupuganti, R. R. et al. N(6)-methyladenosine (m(6)A) recruits and repels proteins to regulate mRNA homeostasis. *Nat. Struct. Mol. Biol.* **24**, 870–878 (2017).
11. Meyer, K. D. et al. Comprehensive analysis of mRNA methylation reveals enrichment in 3′ UTRs and near stop codons. *Cell* **149**, 1635–1646 (2012).
12. Dominissini, D. et al. Topology of the human and mouse m6A RNA methylomes revealed by m6A-seq. *Nature* **485**, 201–206 (2012).
13. Hsu, P. D., Lander, E. S. & Zhang, F. Development and applications of CRISPR-Cas9 for genome engineering. *Cell* **157**, 1262–1278 (2014).
14. Doudna, J. A. & Charpentier, E. Genome editing. The new frontier of genome engineering with CRISPR-Cas9. *Science* **346**, 1258096 (2014).
15. Komor, A. C., Badran, A. H. & Liu, D. R. CRISPR-based technologies for the manipulation of eukaryotic genomes. *Cell* **169**, 559 (2017).
16. Stricker, S. H., Koferle, A. & Beck, S. From profiles to function in epigenomics. *Nat. Rev. Genet.* **18**, 51–66 (2017).
17. Allis, C. D. & Jenuwein, T. The molecular hallmarks of epigenetic control. *Nat. Rev. Genet.* **17**, 487–500 (2016).
18. Liu, X. S. et al. Editing DNA methylation in the mammalian genome. *Cell* **167**, 233–247 e217 (2016).
19. Morita, S. et al. Targeted DNA demethylation in vivo using dCas9-peptide repeat and scFv-TET1 catalytic domain fusions. *Nat. Biotechnol.* **34**, 1060–1065 (2016).
20. Nelles, D. A. et al. Programmable RNA tracking in Live cells with CRISPR/Cas9. *Cell* **165**, 488–496 (2016).
21. O'Connell, M. R. et al. Programmable RNA recognition and cleavage by CRISPR/Cas9. *Nature* **516**, 263–266 (2014).
22. Wang, X. et al. Structural basis of N(6)-adenosine methylation by the METTL3-METTL14 complex. *Nature* **534**, 575–578 (2016).
23. Wang, P., Doxtader, K. A. & Nam, Y. Structural basis for cooperative function of Mettl3 and Mettl14 methyltransferases. *Mol. Cell* **63**, 306–317 (2016).
24. Komor, A. C., Kim, Y. B., Packer, M. S., Zuris, J. A. & Liu, D. R. Programmable editing of a target base in genomic DNA without double-stranded DNA cleavage. *Nature* **533**, 420–424 (2016).
25. Ke, S. et al. m6A mRNA modifications are deposited in nascent pre-mRNA and are not required for splicing but do specify cytoplasmic turnover. *Genes Dev.* **31**, 990–1006 (2017).

26. Linder, B. et al. Single-nucleotide-resolution mapping of m6A and m6Am throughout the transcriptome. *Nat. Methods* **12**, 767–772 (2015).
27. Zhou, J. et al. N(6)-methyladenosine guides mRNA alternative translation during integrated stress response. *Mol. Cell* **69**, 636–647 e637 (2018).
28. Xiao, Y. et al. An elongation- and ligation-based qPCR amplification method for the radiolabeling-free detection of locus-specific N(6)-methyladenosine modification. *Angew. Chem. Int. Ed. Engl.* **57**, 15995–16000 (2018).
29. Liu, Y. et al. Targeting cellular mRNAs translation by CRISPR-Cas9. *Sci. Rep.* **6**, 29652 (2016).
30. Meyer, K. D. et al. 5′ UTR m(6)A promotes cap-independent translation. *Cell* **163**, 999–1010 (2015).
31. Zhou, J. et al. Dynamic m(6)A mRNA methylation directs translational control of heat shock response. *Nature* **526**, 591–594 (2015).
32. Wang, X. et al. N6-methyladenosine-dependent regulation of messenger RNA stability. *Nature* **505**, 117–120 (2014).
33. Liu, N. et al. Probing N6-methyladenosine RNA modification status at single nucleotide resolution in mRNA and long noncoding RNA. *RNA* **19**, 1848–1856 (2013).
34. Zou, S. et al. N(6)-Methyladenosine: a conformational marker that regulates the substrate specificity of human demethylases FTO and ALKBH5. *Sci. Rep.* **6**, 25677 (2016).
35. Mauer, J. et al. Reversible methylation of m6Am in the 5′ cap controls mRNA stability. *Nature* **541**, 371–375 (2017).
36. Wei, J. et al. Differential m(6)A, m(6)Am, and m(1)A demethylation mediated by FTO in the cell nucleus and cytoplasm. *Mol. Cell* **71**, 973–985 e975 (2018).
37. Liu, N. et al. N(6)-methyladenosine-dependent RNA structural switches regulate RNA-protein interactions. *Nature* **518**, 560–564 (2015).

Acknowledgements

We would like to thank Qian laboratory members for helpful discussion. We are grateful to Cornell University Life Sciences Core Laboratory Center for sequencing support. This work was supported by grants to S.-B.Q. from US National Institutes of Health (R01GM122814 and R21CA227917) and HHMI Faculty Scholar (55108556).

Author contributions

S.-B.Q. conceived the project, designed the experiments and wrote the manuscript. X.-M.L. performed most of the experiments and wrote the manuscript. Y.M. conducted the sequencing data analysis. J.Z. contributed to the single nucleotide m^{6}A printing assay and Q.J. helped with data interpretation. All authors discussed the results and edited the manuscript.

Competing interests

The authors declare no competing interests.

Additional information

Supplementary information is available for this paper at https://doi.org/10.1038/s41589-019-0327-1.

Reprints and permissions information is available at www.nature.com/reprints.

Correspondence and requests for materials should be addressed to S.-B.Q.

Publisher's note: Springer Nature remains neutral with regard to jurisdictional claims in published maps and institutional affiliations.

Methods

Cell lines and reagents. MEF, HeLa and HEK293 cells were cultured in Dulbecco's Modification of Eagle's Medium (Corning 10-013-CV) supplemented with 10% fetal bovine serum (Sigma 12306C). Antibodies used in the western blot are listed: anti-ALKBH5 (Millipore ABE1013), anti-FTO (Phosphosolutions 597-Fto), anti-METTL3 (Proteintech 15073-1-AP), anti-Cas9 (Millipore MAC133), anti-HNRNPC (Santa Cruz sc-32308) and anti-β-Actin (Sigma A5441).

Plasmid constructions and PAMmer synthesis. Full-length coding sequences (CDSs) of human *METTL3* and *METL14* were cloned into pcDNA3.1 (Invitrogen) to generate pcDNA-Mettl3 and pcDNA-Mettl14 plasmids. DNA sequences encoding methytransferase domain of METTL3 (residue 369–580) and METTL14 (residue 116–402) were amplified from pcDNA-Mettl3 and pcDNA-Mettl14, respectively, and subcloned into pCMV-BE2 vector backbone (Addgene no. 73020) using Gibson assembly (NEB E2611S). The resulting plasmid was used as a template to produce the methytransferase inactive mutant plasmid (M3^{D395A}M14-dCas9) using Q5 Site-Directed Mutagenesis Kit (NEB E0554S). Full-length coding sequences of human ALKBH5 and FTO were directly cloned into BE2 vector using *Not* I and *Sma* I to generate ALKBH5-dCas9 and FTO-dCas9. The UGI sequences were removed from both vectors. The resulting plasmids were used as templates to generate the demethylase inactive mutant plasmids (ALKBH5H204A-dCas9 and FTOH231A/D233A-dCas9) using Q5 Site-Directed Mutagenesis Kit (NEB E0554S). To purify M3M14 fusion protein from bacteria, M3M14 DNA sequence was amplified from M3M14-dCas9 and subcloned into pGEX-6P-1 vector using *Xho* I and *Not* I. sgRNAs were designed based on the target m^{6}A site for individual RNA and cloned into Cas9 sgRNA vector (Addgene no. 68463). PAMmers were designed based on the principles as previously described[20,21]. The HPLC-purified PAMer sequences consisting of mixed DNA and 2'OMe RNA bases were commercially synthesized by Integrated DNA Technologies. DNA sequences of all primers, sgRNAs and PAMers used in this study are listed in the Supplementary Table 1.

In vitro methylation assay. The RNA probe (5′-CGAUCCUCGGCCAGGACC AGCCUUCCCCAG-3′) derived from *Hsp70* 5′ UTR was commercially synthesized in vitro (Thermo Fisher Scientific). Fusion proteins of M3M14, M14M3 and their catalytically inactive forms were purified from bacteria. The in vitro methylation assay was performed in a 50 µl reaction mixture containing 400 nM RNA probe, 20 mM Tris (pH 7.5), 50 µM $ZnCl_2$, 1 mM DTT, 0.01% Triton X, 0.2 U µl^{-1} RNaseOUT, 1% glycerol, 0.5 µCi (methyl-^{3}H)AdoMet (PerkinElmer) and 100 nM purified protein. The reaction was incubated at 30 °C for 1 h and then stopped by adding Trizol reagent (Invitrogen). RNA after reaction was precipitated and purified using sodium acetate at −20 °C for at least 2 h. The precipitated RNA was subjected to radioactivity measurement using scintillation counting (Beckman). Levels of ^{3}H-methyl-incorporated RNA are shown as disintegrations per minute. The results for methylation assay are shown from four independent replicates.

Cell transfection for RNA m^{6}A editing. MEF or HeLa cells were grown and passaged in a 10-cm culture plate at approximately 80% confluency. For targeted methylation of the m^{6}A sites in exogenously expressed *Hsp70* 5′ UTR-Luc and *Hsp105* 5′ UTR-Luc mRNA, cells were co-transfected with either M3M14-dCas9 or M3^{D395A}M14-dCas9, sgRNA and Fluc reporter plasmids at a mass ratio of 5:3:1 using Lipofectamine 2000 (Life Technologies) according to the manufacturer's guide. For targeted methylation of the endogenous m^{6}A sites of *Hsp105* 5′ UTR and *β-Actin* 3′ UTR cells were co-transfected with M3M14-dCas9 or M3^{D395A}M14-dCas9 and sgRNA at a mass ratio of 5/3 using Lipofectamine 2000. For targeted demethylation of the m^{6}A sites in *Malat1*, cells were co-transfected with ALKBH5-dCas9, FTO-dCas9 or their mutants, and sgRNA plasmids at a mass ratio of 3:1 using Lipofectamine 2000. PAMmers were transfected using Lipofectamine RNAiMax (Life Technologies) according to the manufacturer's instructions. Roughly 36–48 h after transfection, cells were washed with PBS followed by RNA isolation for m^{6}A immunoprecipitation.

m^{6}A immunoprecipitation. Total RNA was isolated using Trizol reagent. Subsequently, the RNA was fragmentized in freshly prepared RNA fragmentation buffer (10 mM Tris-HCl pH 7.0, 10 mM $ZnCl_2$). Then, 180 µg fragmented RNA was incubated with 6 µg anti-m^{6}A antibody in 1× m^{6}A IP buffer (10 mM Tris-HCl pH 7.4, 150 mM NaCl and 0.1% Igepal CA-630) supplemented with 6 µl RNaseOUT (40 U µl^{-1}) and 2 mM RVC for 2 h at 4 °C. The m^{6}A-IP mixture was then incubated with Protein A/G beads and rotated for additional 3 h at 4 °C. Following four washes in 1× IP buffer, m^{6}A-containing RNA fragments were eluted by incubation with 200 µl elution buffer (6.7 mM N^6-methyladenosine 5′-monophosphate sodium salt in 1× IP buffer) for 1 h at 4 °C. Eluted RNA was used for further RT–qPCR.

Immunofluorescence staining. Cells were seeded on glass coverslips at about 70% confluence followed by fixation in 4% paraformaldehyde for 10 min at 4 °C. Subsequently, the fixed cells were treated with 0.2% Triton X-100 at room temperature for 5 min for permeabilization followed by incubation with 1% bovine serum albumin (BSA) for 1 h. After blocking, cells were incubated with anti-Cas9 antibody (Millipore MAC133) overnight at 4 °C and then with Alexa Fluor 546 donkey anti-mouse secondary antibody for 1 h at room temperature. DAPI (1:1,000 dilution)-stained compartments serve as markers of the nuclei. The glass slips were stuck on slides using nail polish and prepared for imaging using a Zeiss LSM710 confocal microscope.

Western blot. Cells were washed twice in PBS and harvested by adding SDS sample buffer (50 mM Tris pH 6.8, 100 mM dithiothreitol, 2% SDS, 0.1% bromophenol blue, 10% glycerol) followed by heating for 10 min at 95 °C. The boiled samples were loaded on SDS–PAGE gels and separated by electrophoresis for about 2 h. The gels were removed from plates and transferred onto Immobilon-P membranes (Millipore) via XCell II Blot Module (Invitrogen). The polyvinylidene difluoride membranes were blocked for 1 h in blocking buffer (1× TBS, 5% non-fat milk and 0.1% Tween-20). Subsequently, the membranes were incubated with primary antibodies overnight at 4 °C followed by blotting with secondary antibodies at room temperature for 1 h. The blotting signal was visualized after reaction with enhanced chemiluminescence (ECL Plus, GE Healthcare).

m^{6}A site-specific detection. Total RNA was isolated from cells 36–48 h after transfection with components for targeted methylation of *Hsp70 5′ UTR* and *β-actin* or demethylation of *Malat1*. In detail, 20 µg total RNA was diluted in 450 µl immunoprecipitation buffer (50 mM Tris, pH 7.4, 100 mM NaCl, 0.05% NP40) and incubated with 1 µg m^{6}A antibody at 4 °C for 2 h, rotating head over tail. The antibody-RNA mixture was then crosslinked twice under the conditions with ultraviolet light at 254 nm 0.15 J cm^{-2} in a Stratalinker (Agilent), followed by precipitation of RNA in 1 ml ethanol and 45 µl sodium acetate. Reverse transcription was performed in a total volume of 7 µl reaction containing m^{6}A-crosslinked RNA, Tth buffer (Promega) and 50 pmole primer. The sequences of the primers targeting m^{6}A sites were listed as follows: Primer targeting *Hspa1a* 5′ UTR, 5′-AGGGATGCTCTGGGGAAGGCTGG-3′; Primer targeting Fluc coding region: 5′-GCGGTCAACGATGAAGAAGTGTTCGTCTTCG-3. Primer targeting *Actb*, 5′-CAAGAAAGGGTGTAACGCAACTAAGTCATAG-3′; Primer targeting *Malat1*, 5′-CAATTAATGCTAGTCCTCAGGATTTAAAAAATAATCTTAACTCAAAG-3′. Subsequently, the reaction mixture was heated at 95 °C for 10 min and gradually cooled to room temperature. Following annealing, 5 U of Tth enzyme and 1 mM $MnCl_2$ were added into the mixture and heated at 70 °C for 3 min. Primer extension was initiated by addition of 1 µM Fluorescein-12-dUTP and reacted for 15 min at 70 °C. The reverse transcription products were resolved on a 15% Novex TBE-urea gels (Thermo Fisher Scientific) and 6-carboxyfluorescein signal was detected by Typhoon 9400 variable mode imager.

SELECT for detection of m^{6}A. Here, 5 µg total RNA was incubated with 40 nM Up Primer, 40 nM Down Primer and 5 µM dNTP in 17 µl 1× CutSmart buffer (50 mM KAc, 20 mM Tris-HAc, 10 mM $MgAc_2$, 100 µg ml^{-1} BSA) and annealed in the programs below: 90 °C (1 min), 80 °C (1 min), 70 °C (1 min), 60 °C (1 min), 50 °C (1 min) and 40 °C (6 min). Subsequently, the 17 µl annealing products were incubated with a 3 µl of enzyme mixture containing 0.01 U Bst 2.0 DNA polymerase, 0.5 U SplintR ligase and 10 nmol ATP. The final 20 µl reaction mixture was incubated at 40 °C for 20 min, denatured at 80 °C for 20 min and kept at 4 °C. Quantitative PCR analysis was carried out as described above and was run under the following conditions: 95 °C, 5 min (95 °C, 10 s; 60 °C, 45 s) for 40 cycles. The SELECT products of indicated site were normalized to the RNA abundance of indicated transcript bearing this site. Primers used in SELECT assay are listed in the Supplementary Table 2.

RT–qPCR. Total RNA was isolated from PBS-washed cells using Trizol reagent. Isolated RNAs were used as templates for reverse transcription based on the manual for High Capacity complementary DNA Reverse Transcription Kit (Invitrogen). Synthesized cDNAs were mixed with Power SYBR Green PCR Master Mix (Applied Biosystems) for qPCR in 384-well plates. The reactions were performed in a LightCycler 480 Real-Time PCR System (Roche Applied Science). Primers used in the qPCR assay are listed in the Supplementary Table 3.

m6A dot blot. RNA was isolated from transfected cells. Equal amounts of RNA were dropped on a nylon membrane (Thermo Fisher Scientific) followed by crosslinking under conditions of ultraviolet light at 254 nm, 0.12 J cm^{-2}. The membrane was blocked in PBS with Tween (PBST) (5% non-fat milk and 0.1% Tween-20) for 1 h and subsequently incubated with anti-m^{6}A antibody (1:1,000 dilution) overnight at 4 °C. After washing three times in PBST buffer, the membrane was blotted with secondary antibody (anti-rabbit, 1:5,000) at room temperature for 1 h. The dot blotting signal was visualized after reaction with enhanced chemiluminescence (ECL Plus, GE Healthcare).

RNA immunoprecipitation. For detection of M3M14-dCas9-sgRNA complex binding to target RNA sequence, HeLa cells were co-transfected with *Hsph1*-Fluc, M3M14-dCas9, control or target sgRNA and increasing dose of PAMer. For detection of HNRNPC binding to *MALAT1*, cells were transfected with target sgRNA, PAMer, control dCas9, ALKBH5-dCas9 or FTO-dCas9. Then, 36 h after transfection, cells were incubated with the growth media containing 1% formaldehyde for 10 min at room temperature, followed by termination

ofthe crosslink reaction by adding 0.25 M glycine (pH 7.5). Then the cells were washed twice with cold PBS and scraped from the plates in cold PBS. The cell suspension was centrifuged at 5,000 r.p.m. for 4 min to pellet the cells. The cell pellets were washed once more and resuspended in 200 µl lysis buffer B (50 mM Tris-HCl pH 7.5, 150 mM KCl, 5 mM EDTA, 1% NP40, 0.1% SDS, 0.5% sodium deoxycholate, 50 mM NaF, protease inhibitor and RNaseOUT) by pipetting up and down. The cell lysate was sonicated for 7 min a Bioruptor sonicator (15 s ON, 30 s OFF), followed by addition of 300 µl RIPA buffer (50 mM Tris-HCl pH 7.5, 150 mM KCl, 1% NP40, 50 mM NaF and protease inhibitor). Insoluble cell debris was pelleted after centrifugation for 10 min at full speed. Normal IgG and Protein A/G bead slurry were added to each 500 µl supernatant to remove non-specific binding. The pre-cleared lysates were incubated with additional 2.5 µl RNaseOUT and Protein A/G bead slurry pre-coated with anti-Cas9 or anti-hnRNP-C antibody at 4 °C for overnight. The beads were washed in RIPA wash buffer (50 mM Tris-HCl pH 7.5, 150 mM KCl, 1% NP40, 0.25% sodium deoxycholate) five times and TE buffer (10 mM Tris-HCl pH 7.5, 1 mM EDTA) another two times. The rinsed beads were then treated with TURBO DNase (Life Technologies) and eluted in RIPA elution buffer (50 mM Tris-HCl pH 7.5, 1 mM EDTA, 10 mM DTT, 1% SDS and RNaseOUT), followed by reverse crosslinking at 70 °C for 5 h and proteinase K digestion. Trizol reagent was added to the bead supernatant to isolate RNA. The RNA was precipitated using isopropanol and reverse transcribed using High Capacity cDNA Reverse Transcription Kit (Invitrogen) using random hexamer primers. Reverse transcription products were used for PCR or qPCR.

Real-time luciferase assay. Cells were grown in 35-mm dishes and transfected with indicated plasmids. Then, 10 min after transfection, firefly luciferase substrate D-luciferin (1 mM, Regis Tech) was added into the culture medium and gently mixed. Luciferase activity was detected in a real-time manner using Kronos Dio Luminometer (Atto).

mRNA stability assay. Cells were treated with transcription inhibitor actinomycin D and collected at different times (0, 1, 3 and 6 h). After washing with PBS, RNA spike-in control (in vitro-synthesized mRNA) and Trizol reagent were added successively to the plates followed by total RNA isolation. After reverse transcription, the mRNA levels of target transcripts were analyzed by qPCR.

m^{6}A-seq. Total RNA was isolated using Trizol reagent followed by fragmentation in RNA fragmentation buffer (10 mM Tris-HCl, pH 7.0, 10 mM $ZnCl_2$). Approximately 400 µg of fragmented RNA was incubated with 6 µg anti-m^{6}A antibody (Synaptic Systems 200 203) and 8 µg anti-m6A antibody Abcam ab151230) in IP buffer (10 mM Tris-HCl, pH 7.4, 150 mM NaCl and 0.1% Igepal CA-630) for 2 h at 4 °C. The antibody-RNA mixture was then incubated with Protein A/G beads for additional 2 h at 4 °C with rotation. After three washes in IP buffer, m^{6}A-containing RNAs were eluted in 100 µl elution buffer (6.7 mM N^6-methyladenosine 5′-monophosphate sodium salt in IP buffer). After ethanol precipitation, eluted RNA was applied for cDNA library construction and high-throughput sequencing.

cDNA library construction. m^{6}A-containing RNAs (m^{6}A-seq) or fragmented total RNAs (RNA-seq) were employed in 15 µl dephosphorylation reaction (20 U T4 polynucleotide kinase, 1× T4 polynucleotide kinase buffer and 10 U SUPERase_In) at 37 °C for 1 h. The dephosphorylated RNAs in the size range 40–60 nt were sliced and disrupted after separation a 15% polyacrylamide TBE-urea gel (Invitrogen). The disrupted gels containing RNA fragments were immersed in 400 µl gel elution buffer (1 mM EDTA, 300 mM NaOAc, pH 5.5 and 0.1 U ml^{-1} SUPERase_In) at 4 °C overnight with rotation. After removal of gel debris using a Spin-X column (Corning), the RNAs were precipitated in ethanol followed by resuspension in nuclease-free water. Poly-(A) tails were then added to the purified RNAs at 37 °C for 45 min in the reaction containing 1× poly-(A) polymerase buffer, 3 U *E. coli* poly-(A) polymerase, 1 mM ATP and 0.75 U µl^{-1} SUPERase_ In. Subsequently, the polyadenylated RNAs were used as templates for reverse transcription. Listed below are barcoded primers used for reverse transcription:

MCA02: 5′-pCAGATCGTCGGACTGTAGAACTCTCAAGCAGAAGACGGC ATACGATTT TTTTTTTTTTTTTTTTTVN-3′

LGT03: 5′-pGTGATCGTCGGACTGTAGAACTCTCAAGCAGAAGAC GGCATACGATT TTTTTTTTTTTTTTTTTVN-3′

YAG04: 5′-pAGGATCGTCGGACTGTAGAACTCTCAAGCAGAAGACG GCATACGATT TTTTTTTTTTTTTTTTTVN-3′

HTC05: 5′-pTCGATCGTCGGACTGTAGAACTCTCAAGCAGAAGAC GGCATACGATT TTTTTTTTTTTTTTTTTVN-3′

The reverse transcription was performed by initial incubation of polyadenylated RNAs with 2.5 mM synthesized primer and 0.5 mM dNTP at 65 °C for 5 min. After cooling on ice for 5 min, the primer extension was carried out by incubation of the annealing products with 200 U SuperScript III, 20 mM Tris (pH 8.4), 5 mM $MgCl_2$, 50 mM KCl, 10 mM DTT and 40 U RNaseOUT. The detailed procedures were described in the manufacturer's instruction. cDNA products were separated on a 10% polyacrylamide TBE-urea gel (Invitrogen). The products in the size range 100–150 nt were excised and released in DNA gel elution buffer (300 mM NaCl, 1 mM EDTA). The precipitated and eluted cDNAs were then circularized at 60 °C for 1 h in a 20 µl of circularization reaction (100 U CircLigase ssDNA Ligase, 1× CircLigase buffer, 50 mM ATP and 2.5 mM $MnCl_2$) (Epicentre). The circularized products served as templates for PCR.

Deep sequencing. Circularized products were used as templates for PCR reactions catalyzed by the Phusion High-Fidelity enzyme (NEB). The PCR was performed in a 20 µl reaction (1× HF buffer, 0.2 mM dNTP, 0.5 µM forward and reverse primers and 0.5 U Phusion polymerase) using primers qNTI200 (5′-CAAGCAGAAGACGGCATA-3′) and qNTI201 (5′-AATGATACGGCGACC ACCG ACAGGTTCAGAGTTCTACAGTCCGACG-3′). PCR was run under the following conditions: 98 °C, 30 s; (98 °C, 10 s; 60 °C, 20 s; 72 °C, 10 s) for 12 cycles; 72 °C, 10 min. Subsequently, the PCR products with expected size 140 base pairs were excised after separation on a 8% polyacrylamide TBE gel (Invitrogen). The DNA products were recovered from DNA gel elution buffer followed by quantification using Agilent BioAnalyzer DNA 1000 assay. The equal amounts of barcoded samples were pooled together and used for cluster generation followed by deep sequencing (Illumina HiSeq). The sequencing primer was 5′-CGACAGGTTCAGAGTTCTACAG TCCGACGATC-3′.

m^{6}A peak calling. The sequencing reads, after trimmed 3′ adaptor and low-quality bases, were aligned to human transcriptome, using Bowtie with parameters: -a —best -m1 —strata. The annotation file downloaded from ENSEMBL database (GRCh38) was used to construct the transcriptome index file. For each gene, the transcript with the longest CDS was selected. In the case of equal CDS length, the longest transcript was used. For read alignment, a maximum of two mismatches were permitted. To avoid ambiguous, the reads mapped to multiple positions were disregarded for further analyses.

We used a non-parameter method to predict m^{6}A sites on transcripts. In brief, a sliding window of 50 nt with a step of 25 nt was employed to scan each transcript. For each window with maximum read coverage higher than ten, a peak-over-median score (POM) was derived by calculating the ratio of the mean read coverage in the window to the median read coverage of corresponding transcript. The windows with a POM higher than three in an IP sample were obtained. The same processes were performed in input sample. The windows found in input sample were eliminated from following analyses. The windows that overlapped at least single nucleotide were merged into one cluster. Finally, a peak-over-input score was assigned to each cluster by calculating the ratio of POM in the IP sample to that in the input sample. The cluster with peak-over-input score higher than three were retrieved, and defined as an m^{6}A-enriched cluster. The peak position with maximum coverage in each m^{6}A-enriched cluster was defined as the position of m^{6}A peak. The adenosine site of the nearest RRAC motif was defined as m^{6}A residue. To reduce noises for background reads and bias from peak calling method, only the m^{6}A sites that were found in all biological replicates were used. The coverage of m^{6}A site was defined as the reads per kilobase million value surrounding m^{6}A sites from −50 to +50 nt.

Reporting Summary. Further information on research design is available in the Nature Research Reporting Summary linked to this article.

Data availability

All sequencing raw data and processed files have been deposited in the Gene Expression Omnibus (GSE132051).

nature research

Corresponding author(s): Shu-Bing Qian
NCHEMB-A180507654-B

Reporting Summary

Nature Research wishes to improve the reproducibility of the work that we publish. This form provides structure for consistency and transparency in reporting. For further information on Nature Research policies, see Authors & Referees and the Editorial Policy Checklist.

Statistical parameters

When statistical analyses are reported, confirm that the following items are present in the relevant location (e.g. figure legend, table legend, main text, or Methods section).

n/a	Confirmed	
☐	☒	The exact sample size (*n*) for each experimental group/condition, given as a discrete number and unit of measurement
☐	☒	An indication of whether measurements were taken from distinct samples or whether the same sample was measured repeatedly
☐	☒	The statistical test(s) used AND whether they are one- or two-sided *Only common tests should be described solely by name; describe more complex techniques in the Methods section.*
☒	☐	A description of all covariates tested
☒	☐	A description of any assumptions or corrections, such as tests of normality and adjustment for multiple comparisons
☐	☒	A full description of the statistics including central tendency (e.g. means) or other basic estimates (e.g. regression coefficient) AND variation (e.g. standard deviation) or associated estimates of uncertainty (e.g. confidence intervals)
☐	☒	For null hypothesis testing, the test statistic (e.g. *F*, *t*, *r*) with confidence intervals, effect sizes, degrees of freedom and *P* value noted *Give P values as exact values whenever suitable.*
☐	☒	For Bayesian analysis, information on the choice of priors and Markov chain Monte Carlo settings
☒	☐	For hierarchical and complex designs, identification of the appropriate level for tests and full reporting of outcomes
☒	☐	Estimates of effect sizes (e.g. Cohen's *d*, Pearson's *r*), indicating how they were calculated
☐	☒	Clearly defined error bars *State explicitly what error bars represent (e.g. SD, SE, CI)*

Our web collection on statistics for biologists may be useful.

Software and code

Policy information about availability of computer code

Data collection	Firefly luciferase activities were collected by Luciferase Reporter Assay System (Promega). qPCR assays were carried on a LightCycler 480 Real-Time PCR System (Roche Applied Science). Immunoblots were performed using enhanced chemiluminescence (ECL plus, GE Healthcare). Immunofluorescence imaging was performed using a Zeiss LSM710 confocal microscope. High through-put sequencing data was collected by illumina HiSeq Control Software v2.2.58 for HiSeq2500 System.
Data analysis	Graphpad Prism, SigmaPlot, Adobe Illustrator, Cutadapt v1.18 , Bowtie v1.1.2, R v3.5.1, Custom Perl scripts (RNA-seq and m6A-seq data) are available on request to the corresponding authors.

For manuscripts utilizing custom algorithms or software that are central to the research but not yet described in published literature, software must be made available to editors/reviewers upon request. We strongly encourage code deposition in a community repository (e.g. GitHub). See the Nature Research guidelines for submitting code & software for further information.

Data

Policy information about availability of data

All manuscripts must include a data availability statement. This statement should provide the following information, where applicable:

- Accession codes, unique identifiers, or web links for publicly available datasets
- A list of figures that have associated raw data
- A description of any restrictions on data availability

The data that support the findings of this study are available from the corresponding author upon reasonable request.

Field-specific reporting

Please select the best fit for your research. If you are not sure, read the appropriate sections before making your selection.

☒ Life sciences ☐ Behavioural & social sciences ☐ Ecological, evolutionary & environmental sciences

For a reference copy of the document with all sections, see nature.com/authors/policies/ReportingSummary-flat.pdf

Life sciences study design

All studies must disclose on these points even when the disclosure is negative.

Sample size	Sample sizes are indicated in the figure legends.
Data exclusions	No data was excluded.
Replication	Experimental findings were reliably reproduced.
Randomization	Randomization was not performed in our studies.
Blinding	Blinding was not used in our studies.

Reporting for specific materials, systems and methods

Materials & experimental systems

n/a	Involved in the study
☒	☐ Unique biological materials
☐	☒ Antibodies
☐	☒ Eukaryotic cell lines
☒	☐ Palaeontology
☒	☐ Animals and other organisms
☒	☐ Human research participants

Methods

n/a	Involved in the study
☒	☐ ChIP-seq
☒	☐ Flow cytometry
☒	☐ MRI-based neuroimaging

Antibodies

Antibodies used	anti-ALKBH5 (Millipore ABE1013), anti-FTO (Phosphosolutions 597-Fto), anti-METTL3 (Proteintech 15073-1-AP), anti-Cas9 (Millipore MAC133), anti-HNRNPC (Santa cruz sc-32308) and anti-β-Actin (Sigma A5441), anti-m6A (Synaptic Systems Cat#202 003), anti-m6A (Millipore Cat#ABE572), Anti-m6A (Abcam, ab151230).
Validation	Antibodies were validated by the suppliers.

Eukaryotic cell lines

Policy information about cell lines

Cell line source(s)	Mouse embryonic fibroblast cell (MEF) was provided by the Laboratory of David J. Kwiatkowski. HeLa cells were puchased from the American Type Culture Collection (ATCC).

Authentication	No method of cell line authentication was used.
Mycoplasma contamination	Cell lines were not tested for mycoplasma.
Commonly misidentified lines (See ICLAC register)	No commonly misidentified cell lines were used.